



Mechanics of granular and polycrystalline solids

Influence of the morphology of slope and blocks on the energy dissipations in a rock avalanche



Influence de la morphologie de la pente et des blocs sur les modes de dissipation d'énergie dans une avalanche rocheuse

Dominique Daudon*, Pascal Villard, Vincent Richéfeu, Guilhem Mollon

Université Grenoble-Alpes, 3SR Lab, 175, rue de la Passerelle, 38400 Saint-Martin-d'Hères, France

ARTICLE INFO

Article history:

Received 17 January 2014

Accepted 4 July 2014

Available online 19 December 2014

Keywords:

Rock avalanches

Discrete elements

Mechanical dissipation

Sensitivity study

Granular flows

Mots-clés :

Avalanches rocheuses

Éléments discrets

Dissipation mécanique

Étude de sensibilité

Écoulement granulaire

ABSTRACT

A discrete element model was used to determine the influence of block shape and surface topography on energy dissipative modes occurring during rockfalls or avalanches. By using realistic shapes of particles and a specific contact law able to represent the main dissipation phenomena at the contact-rebound point, we analyze the contribution of tangential and collisional effects within the granular material or at the base of the flow. It was shown that the particle shape and the slope geometry have a major influence on the energy dissipative modes and need to be accounted for in numerical models.

© 2014 Published by Elsevier Masson SAS on behalf of Académie des sciences.

RÉSUMÉ

Les modes de dissipations énergétiques lors de la propagation d'avalanches de roches sont étudiés à l'aide d'un modèle numérique aux éléments discrets. En utilisant des formes de blocs réalistes et une loi de contact spécifique permettant de prendre en considération les principaux phénomènes dissipatifs qui surviennent lors d'un impact, il nous a été possible d'analyser les différents modes de dissipation, par frottement et par chocs, qui se développent au sein du matériau granulaire ou à la base de l'écoulement. Il est montré que la forme des particules et la géométrie de la pente ont une influence majeure sur les modes de dissipation d'énergie et doivent être pris en compte dans les modèles numériques pour une meilleure prédition de la propagation des avalanches rocheuses.

© 2014 Published by Elsevier Masson SAS on behalf of Académie des sciences.

1. Introduction

Rock avalanches are among the most frequent and unpredictable natural events that need to be taken into account to define the risks in the mountainous infrastructures. The complexity of the interacting mechanisms involved during the flow has a great influence on the morphology of the deposit and on the propagation distance of a rock mass. The nature of the

* Corresponding author.

E-mail address: dominique.daudon@3sr-grenoble.fr (D. Daudon).

flow patterns and the mode of interaction between blocks strongly depend on the shape, size, and number of blocks as well as the geometry of the surface topography. The influence of these parameters on the kinematics of the flow and on the amounts of energy dissipated at the base and within the moving granular mass is one of the key points that must be raised in order to predict satisfactorily the propagation and deposition areas of the granular mass.

Usually, the trajectory of individual block and the position of the stop zone are approximated using softwares based on mass-point mechanics for which the energy dissipation at each contact depends on damping and frictional coefficients [1–3]. Small avalanches may be studied with a probabilistic approach of the precedent trajectory methods [4,5], but energy dissipation is modeled through restitution coefficients, defined in normal or/and tangential directions, which may be expressed either with velocity ratios or kinetic energy ratios [6,2,7–10]. Some authors have shown that the kinetic of the impact depends strongly on the substrate nature related to soft or hard contacts [11,12,1,3], on the shape of the blocks and on the impact angle [6,10,13,14]. So, different values and definitions of the restitution coefficient are proposed in the literature, leading in some cases (transformation of rotational energy into translation energy for example) to unphysical values greater than the unity limit [15].

Larger avalanches are generally modeled with fluid-like engineering softwares based on the assumption of a shallow water fluid behavior. This type of hypothesis leads to a smoothing of the internal fluid phenomena such as re-circulation or velocity fluctuations. The frictional dissipative mechanisms are generally located at the basal interaction between fluid and substrate, or averaged in the fluid [16–19]. The parameters are obtained from laboratory studies [20,17,21] or more often from back-analysis of real cases.

Nevertheless, none of these two types of model is completely satisfactory, specifically for medium volume avalanches where interactions between particles cannot be ignored while the mass is discontinuous in some place. In fact, the complex collective behavior between particles such as collision, friction, transfers of translation velocity to rotational velocity are not represented with the mass center point mechanics trajectory. Besides, the shallow-water continuous model, although commonly used in the communities of stakeholders and researchers, cannot account for some mechanical effects, especially at the change in slope geometries, without adding numerical specific ingredients [19,22].

In this context, the discrete element modeling offers an interesting alternative to the continuous approaches as, using specific assumptions on the constitutive contact law and real representation of the block shapes, they seem to be more relevant in modeling medium and small volumes of rock avalanches [23–29]. The contact law between particles becomes a factor of importance in this case. In general, the classical elastic laws with friction are used [30,31,27] and some dissipation parameters may be added as in Walton's laws [32,33]. The particles' shape may be taken into account by using polygons [31], spheres, clumps of spheres, ellipsoids, spheropolyhedrons [34].

The model proposed here is able to take into account realistic block shapes [35] and is based on the definition of specific interaction laws that make physical parameters easily assessable by means of a simple laboratory experiment of block launch retro-analysis [36]. Each block is modeled by a spheropolyhedron, which is the shape resulting from the sweeping of a sphere onto the surface of a polyhedron [37]. This makes it possible to obtain realistic shapes, to optimize the contact detection algorithm and to minimize the time calculation. The contact model, described in the following section, is tested and validated with laboratory experiments performed at EPFL [38], which consist in the release of an assembly of small bricks on a bi-plane. Then, the model is used to highlight the energy dissipation mechanisms occurring along the slope, especially the influence of the blocks shape (bricks and cubes), the undulation of the slope, and the effect of the slope transition between the two planes.

2. Contact law and calibration of parameters

The quality of a numerical model is partly linked to its ability to reproduce and predict a physical phenomenon and secondly to the ease with which the user is able to identify the parameters. The contact model that we used to simulate the dissipative mechanisms occurring during an impact between two solids is deliberately minimalist and defined by four parameters that can be easily identified by laboratory tests (e_n^2 , μ , k_n and k_t).

The parameter e_n^2 reflects the amount of energy restored in the direction perpendicular to the contact plane at each cycle of loading/unloading of the contact. In the case of a vertical drop of a particle on a horizontal plane, this coefficient is the ratio between the height of rebound of the particle and the height of the initial drop. A value of 1 corresponds to a perfectly elastic collision and a value close to 0 refers to a completely dissipative contact. As shown by many authors, this coefficient depends on the impact velocity and on the impact angle [39,40,42–44]. In the laboratory experiments presented in this paper, the range of normal velocities at collision is relatively narrow. This makes the parameter e_n^2 nearly constant, in fact [41]. Actually, this parameter integrates a very complex set of mechanisms that are difficult to identify (damage, plastification, elastic wave, heat generation, etc.). From this point of view, the chosen behavior law does not include the actual mechanisms of energy dissipation, but allow in a comprehensive manner, by using a simplified contact law, to access to the amount of energy dissipated during impact.

The parameter μ is a coefficient that introduces energy dissipation in the tangential direction to the contact plane. Upon contact between two rigid bodies, this parameter is the dynamic friction coefficient. For a contact between a boulder and loose soil, this coefficient incorporates, in addition to frictional forces, the abutment force and the shear strength of the soil of the impacted area. However, it behaves exactly like a classical Coulomb friction coefficient.

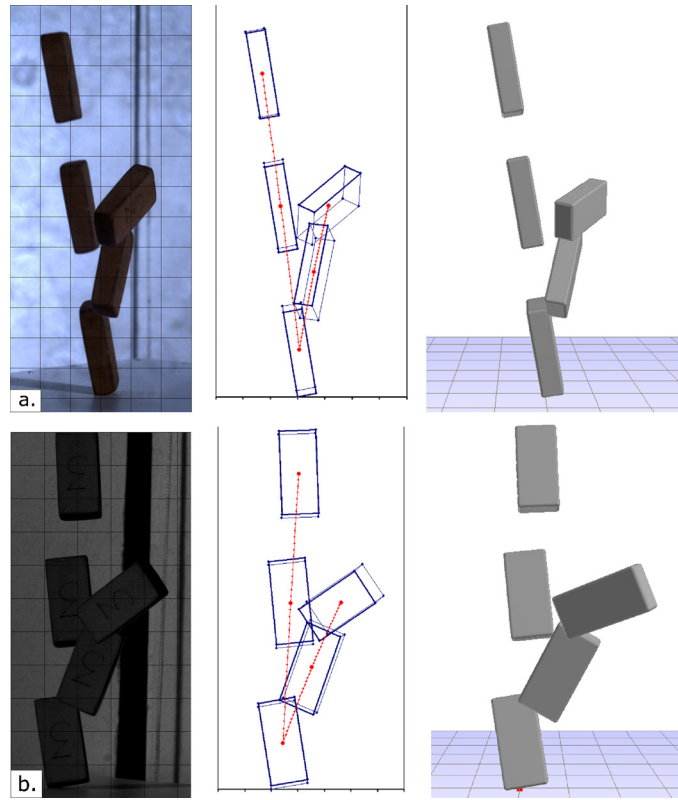


Fig. 1. (Color online.) Principle of the parameters identification procedure: (a) color camera 1; (b) B&W camera 2.

The parameters k_n and k_s are respectively associated with the stiffness of the contact in the normal and tangential directions. During contact between two particles, the normal and tangential forces of interaction $F_n(t)$ and $F_t(t)$ are calculated incrementally at each time step δt based on the normal interpenetration h_n between particles and on their normal and tangential velocities (\dot{h}_n and \dot{h}_t); Eqs. (1) and (2). Note that the tangential force is formally written as in two-dimensional case for a sake of simplicity:

$$\begin{cases} F_n(t + \delta t) = F_n(t) + k_n \dot{h}_n \delta t & \text{if } \dot{h}_n \geq 0 \\ F_n(t + \delta t) = e_n^2 k_n h_n & \text{if } \dot{h}_n < 0 \end{cases} \quad (1)$$

$$F_t(t + \delta t) = \min(F_t(t) + k_t \dot{h}_t \delta t; \mu F_n(t)) \quad (2)$$

Eq. (1) reflects the fact that the energy dissipated in the normal direction of the contact during a cycle of loading/unloading is the difference between the energy stored during the impact (as a function of k_n) and the energy restored to the particle during unloading (as a function of $e_n^2 k_n$). The value of the normal stiffness parameter k_n affects the interpenetration distance, the contact duration, and the value of the maximum impact force, but not the proportion of dissipated energy that is invariably of e_n^2 .

The interaction forces in the tangential direction to the contact plane (Eq. (2)) are governed by Mohr–Coulomb elastic–plastic law. The tangential stiffness parameter k_t has a key role in the speed at which the threshold tangential force is reached. This force is proportional to the coefficient μ and to the normal force F_n at the contact point.

For a relevant modeling and a correct estimation of the dissipated energy, the time step δt must be sufficiently small. For the cases studied, 40 to 50 calculation steps are needed to adequately describe an impact.

To carry out the modeling of the experiments performed at EPFL [38], we have implemented a specific procedure, currently operational in laboratory, to identify the numerical contact parameters. This procedure consists in analyzing the fall and rebound of a single particle on a horizontal plane, using a device consisting of two synchronized high-speed cameras shooting at 1000 fps.

Several impact tests between brick/support and brick/brick were performed. The materials needed for experiments (bricks and support), identical to those used at EPFL [38], have been made available to us as part of the European project Alcotra MASSA. The analysis of several rebounds allows optimizing the values of the numerical parameters by using an error function that characterizes the difference between the actual trajectory of the particle, before and after rebound, and the one restored by the numerical model. It was supposed that the impact velocity and the localization of the impact (corners, edges or faces) have a minor influence on the values of the contact parameters.

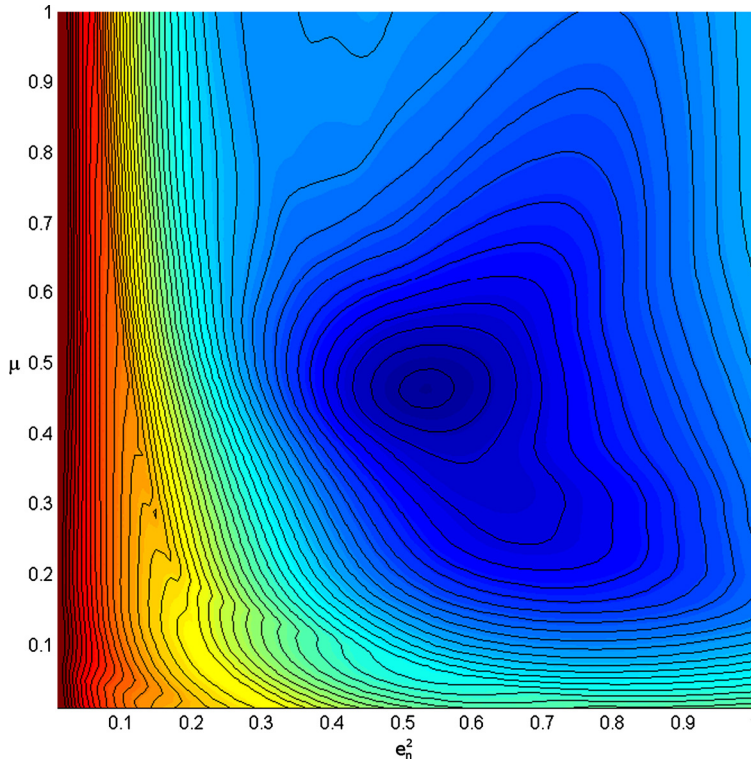


Fig. 2. (Color online.) Isovalue-curves of the error function (which is a summed-squared-distances between simulated trajectories and those identified from experiments) associated with the parameters ϵ_n^2 and μ (brick/support interaction). The optimization was performed for the four contact parameters simultaneously from a series of collisions between two bricks or between a brick and the same support used in experiments [35].

Table 1
Optimal parameters obtained by minimizing the error function.

	ϵ_n^2	μ	k_n	k_t/k_n
Brick/support	0.53	0.46	10^5	0.42
Brick/brick	0.13	0.86	10^5	0.27

An illustration of this procedure, applied to the two cameras, is shown in Fig. 1 for one of the performed tests. The pictures on the left correspond to the some images taken by the camera at a regular time step of 20 ms, the pictures in the center correspond to the trajectories identified after analysis of camera images, those on the right correspond to the numerical trajectories recalculated by using the optimized parameters obtained by the study of several rebounds.

The optimization procedure consists in varying the four numerical parameters and in calculating, for each set of parameters, an error function based on the comparison between the actual trajectories of particles (sampled every ms from the high-speed cameras) and those returned by the numerical model. As an example, we present in Fig. 2 the isovalue curves of the error function associated with the parameters ϵ_n^2 and μ , which are the most influent parameters to restore the trajectory after the impact. The central part of Fig. 2 characterizes the area for which the error function is minimized for the parameters ϵ_n^2 and μ . By plotting for each couple of parameters the error function, it is possible to identify an optimum set of parameters. The values obtained for the brick/support or brick/brick interactions are given Table 1. For more details on the identification process of the experimental trajectories or on the definition of the error function, the reader can refer to the work presented in [35].

3. Validation of the numerical model

After calibration of the contact parameters, the robustness of the numerical model was validated by comparison with small-size laboratory experiments implementing an assembly of small bricks (size of 31 mm × 15 mm × 8 mm) propagating along an inclined slope and then stopping on a horizontal plane. The advantage of such simulations is to test the ability of the numerical model to predict the collective flow of a granular mass, based on contact parameters obtained by studying the bounce of a single particle.

On the other hand, this makes it possible to understand, by calculating variables that are difficult to measure, what are the key parameters influencing the kinematics of the flow and the final position of the granular deposit. The influence of

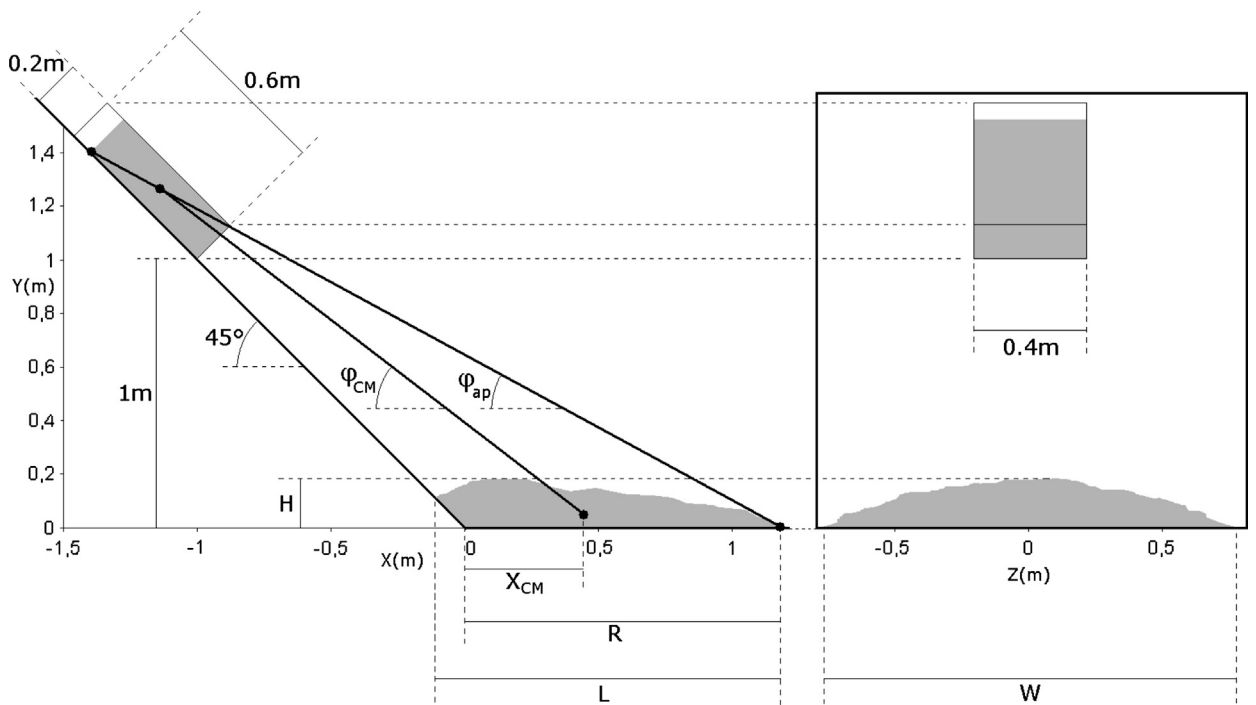


Fig. 3. Scheme of the experimental device and description of the geometric parameters.

Table 2

Geometric characteristics of the position and shape deposit with errors relative to the experimental values.

	H (m)	L (m)	W (m)	R (m)	φ_{CM} (°)	φ_{app} (°)	X_{CM} (m)
Experimental	0.075	0.930	1.400	0.840	40.0	32.0	0.370
Numerical	0.120	0.882	1.383	0.824	40.1	32.2	0.332
Relative error (%)	+60.00	-5.16	-1.21	-1.90	+0.25	+0.62	-10.27

the particle shape and of the topography geometry on the modes of energy dissipation (at the base or within the flow, by shocks or friction) is one of the challenges of the work presented in the following section of this paper.

The experiment used for the validation of the numerical model consists in the release and the flow on an inclined plane of 6300 small bricks randomly poured in a starting box (size of $0.2 \text{ m} \times 0.4 \text{ m} \times 0.6 \text{ m}$). Among the experiments of the literature, it was chosen because of its simple geometric configuration (boundary conditions, exact number, shape, and size of the particles). Also, the material needed to determine the contact parameters was obtained through a collaboration established as part of European project Alcotra MASSA. Fig. 3 provides the geometry of the experimental tests and the definition of the main parameters. The bricks are launched at a height of 1 m on a slope of smooth plastic material inclined at 45° , ending on a planar horizontal deposit zone. The numerical contact parameters are those obtained after the calibration process. The experimental characteristics of the deposit zone (i.e. dimensions, position, shape) are measured by an optical technique [38]. Numerically, specific algorithms have been developed to define the geometry of the deposit and some characteristics of the kinematics of the flow (average speed and front velocity of the flow).

The comparisons between the physical experiments and the numerical model, presented in Table 2, are based on the characteristics of the granular deposit (size, position of the centre of gravity) and on quantities typically measured in the framework of rockfalls (so-called Fahrböschung angle φ_{app} and travel angle φ_{CM}). As can be seen in Table 3, the comparison between the numerical and experimental deposit shapes is satisfactory, in terms of horizontal dimensions and somewhat less in terms of height (relative error of 60%). In particular, the position X_{CM} of the center of mass of the deposit is correctly assessed (0.33 m against 0.37 m for experimental work, i.e. a relative error of about 10%). In the same way, the travel angle φ_{CM} related to the center of mass and the angle φ_{app} related to the extreme points of the granular deposit are very accurately reproduced as rather same values of $\varphi_{CM} = 40^\circ$ and $\varphi_{app} = 32^\circ$ were obtained. The differences between the height of the granular deposit are attributed to the difficulty to measure experimentally and to define numerically the shape deposit on the basis of discrete particles (the height estimated numerically corresponds to the one of the highest particle, while the experimental one is obtained by optical techniques that introduce an undefined amount of smoothing of the deposit surface).

Although the contact model has been calibrated through the study of an elementary rebound, it is probably not possible to predict the trajectory of a single particle during multiple rebounds, given the slight imperfections in shape particle and

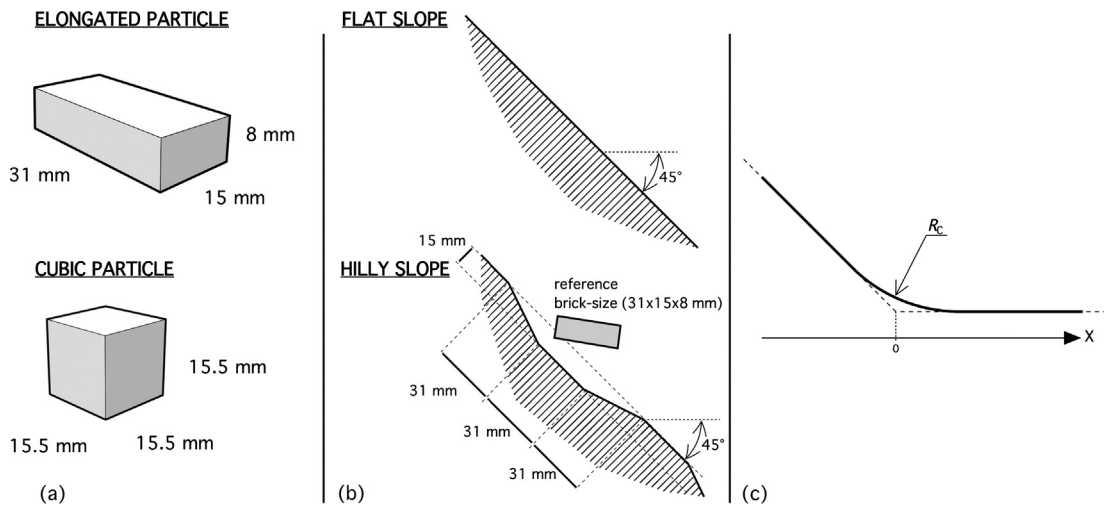


Fig. 4. Geometric features that have been changed to get a sense of their role: (a) shapes aspect ratio, (b) slope undulations, (c) rounding of the slope transition.

the approximations made when determining the contact parameters. The comparison between experiment and modeling on a collective release of particles shows, however, that due to multiple interactions between particles within the flow, it is possible to approach very satisfactorily the main features of the deposit. Imperfections in brick shape or uncertainties on the contact parameters have consequently little influence on the collective behavior of the granular mass. Given the good agreement between the numerical and experimental deposit positions, it is likely that the energy dissipation mechanisms have been properly modeled. Knowing the contact forces and the relative displacements between the particles themselves or with the support, it is possible to identify the contact force work and to deduce the amount of energy dissipated at each time step, either within the granular mass or at the base of the flow. The next section will be devoted to the influence of the particle shape and of the geometry of the slope on the energy dissipation mechanisms (undulated slope or curved section at the transitional area between the slope and the horizontal plane).

4. Influence of morphological parameters

The model being validated, it is now possible to study further the influence of different factors on the dissipation modes and locations during the flow, and the resulting morphology of the deposit. In this section, the focus is on how the avalanche is affected by (i) the aspect ratio of the block shape, (ii) the presence of block-sized undulations onto the slope, and (iii) a less steep transition in the slope gradient at the device toe. These three changes concern only geometric features, and the mechanical parameters are deliberately kept the same; for a sensitivity study of the contact parameters, the interested reader may refer to [36]. For the present analysis, we will use as a reference the simulation of brick release previously validated, and compare it with other simulations for which only one geometric parameter (block shape, slope undulation or transition curvature) is modified at a time (Fig. 4).

4.1. Aspect ratio of the blocks

The role of the aspect ratio of the blocks is regarded by comparing the reference release of elongated bricks (aspect ratio of about 2) with the release of cubes. Bricks and cubes have the same volume; see Fig. 4a. A particular attention was paid to analyze the dissipative energy mechanisms occurring at different areas of the flow. The dissipated energy at the base of the flow was computed considering the normal and tangential contact forces and relative displacements between blocks and slope while the dissipated energy within the flow was obtained by taking into account contact forces and displacements between blocks. The type and localization of the cumulated energy dissipations for the avalanche of bricks and cubes are shown in Figs. 5a and 5b. Three zones of spreading are considered on the device. Zone 2, surrounding the change in gradient, separates the slope (zone 1) from the stop area (zone 3). Also, four modes of dissipation (work of contact forces by unit horizontal length along the propagation direction) are distinguished, namely the dissipation by collisions with the support W_n^{BS} , by collisions in-between the particles W_n^{BB} , by friction with the support W_t^{BS} , and by friction within the mass W_t^{BB} . For each case, a view of the final deposit is shown on the same figure where the particles are colored as a function of their altitude.

When compared with the release of bricks, a noticeable difference with cubes deals with the final position of the blocks (deposit and isolated particles) and on the dissipative energy modes. In particular, it can be seen that, whatever the zone, most of the energy was dissipated within the bulk for the cubes, while most of the energy was dissipated by friction for the bricks. In other word, the granular flow involving bricks was disturbed by the collisional movement of the particles, while

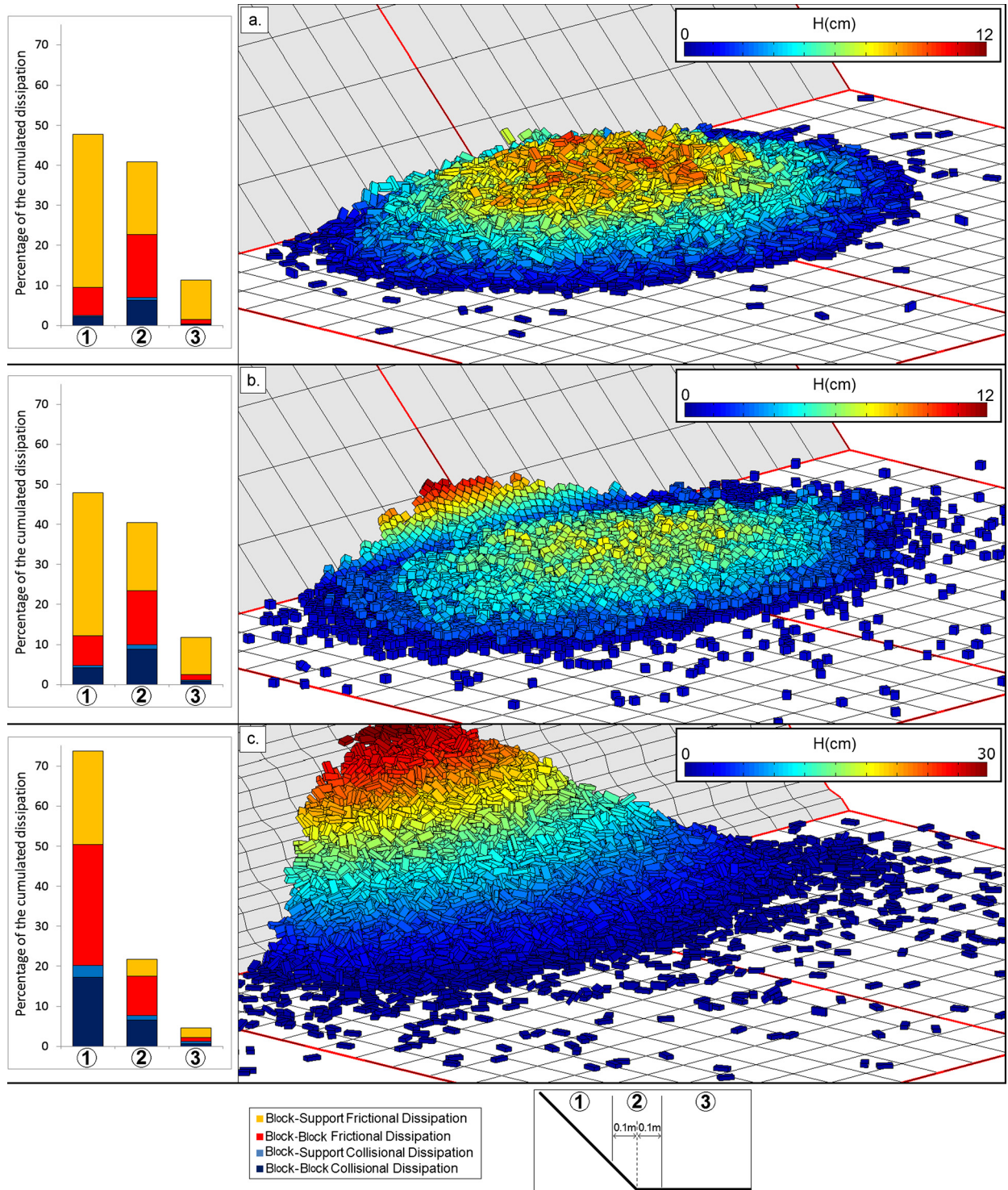


Fig. 5. (Color online.) (Left) Energy dissipation cumulated from initiation to the stop times in slope, transition and stop area as a function of their type and (right) screenshot of the deposit for (a) the reference simulation with bricks on flat slope, (b) cubes on flat slope and (c) bricks on hilly slope. The particles' colors correspond to their altitudes.

Table 3

Main characteristics of the deposits for releases of bricks and cubes on flat slope, and bricks on hilly slope.

	R (m)	L (m)	W (m)	φ_{CM} ($^{\circ}$)	φ_{app} ($^{\circ}$)
Bricks on flat slope	0.84	0.91	1.37	31.5	40.1
Cubes on flat slope	0.76	0.84	1.40	32.3	40.2
Bricks on hilly slope	0.48	0.81	1.48	36.0	45.5

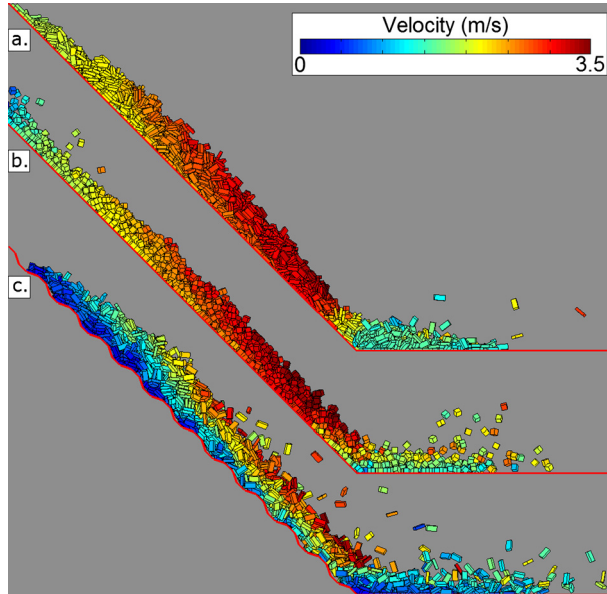


Fig. 6. (Color online.) Lateral view of the particle velocities soon after the mass crossed the transition for the reference simulation (a), cubes on flat slope (b) and bricks on hilly slope (c).

the bricks have a greater tendency to slip, which promotes the dissipation by friction both in the mass and at the base of the flow. This might also be explained by the greater rolling ability of cubes compared to bricks. This feature induces a slight increase in the number of collisions in the area of disturbance of the flow, and causes at the same time a limited reduction of the energy dissipated by friction at the base of the transition zone. This can be especially noted for the transitional zone (zone 2) for which the flow was mostly disturbed.

However, it is interesting to notice that the total amount of energy dissipated in each zone seems not be significantly affected by the aspect ratio of the blocks (provided that the aspect ratio is not too high, like in the present case). In our case, because of a greater ability to roll and given the chosen dissipation parameters (e_n^2 and μ), the energy dissipated by collisions (light and dark blue in Fig. 5a) is higher for the cubes than for the bricks in the zones 1 and 2. As a consequence, the energy dissipated by collisions during the rolling of cubes on the stop zone is higher than the energy dissipated by friction during the sliding of the bricks on the same zone, which explains the longer run-out distance for the reference release with bricks.

The mean geometrical characteristics of the deposit are given in Table 3 and illustrated in the screenshots of Figs. 5a and 5b. It can be seen that, despite an equal amount of energy dissipated in each zone, the two deposits have significant differences. A cubic shape leads to a smaller deposit length and run-out distance, and a larger deposit width despite a larger spreading of the isolated particles. This indicates that the manner the energy is dissipated, that is mainly by friction or by collisions, has strong consequences on the efficiency of the mass stop. It can be noted that the scattering of the isolated cubes is also a consequence of the greater rolling ability of cubes compared to bricks. It is important to stress here that the results obtained are highly dependent on the dissipation parameters and cannot be generalized. One can however remark that both the shape of the blocks and the dissipation parameters play key roles on the rheological behavior of an avalanche.

4.2. Bumpy terrain

The role of block-sized ripples on the propagation slope is regarded by comparing the result of the reference release with a similar case differing only by the “keystoned” undulations of the slope (Fig. 4b). The dissipated energy in the three zones previously defined can be compared in Figs. 5a and 5c. As we can see, the ripples in the slope play a crucial role in mass propagation. In particular, the runout distance is clearly shorter due to more dissipated energy in the bumpy slope (see Table 3). By looking more specifically at the dissipation modes in each zone, it is observed that the energy loss is incremented in the slope by an increase of collisions and friction between the blocks. This is a direct result of the

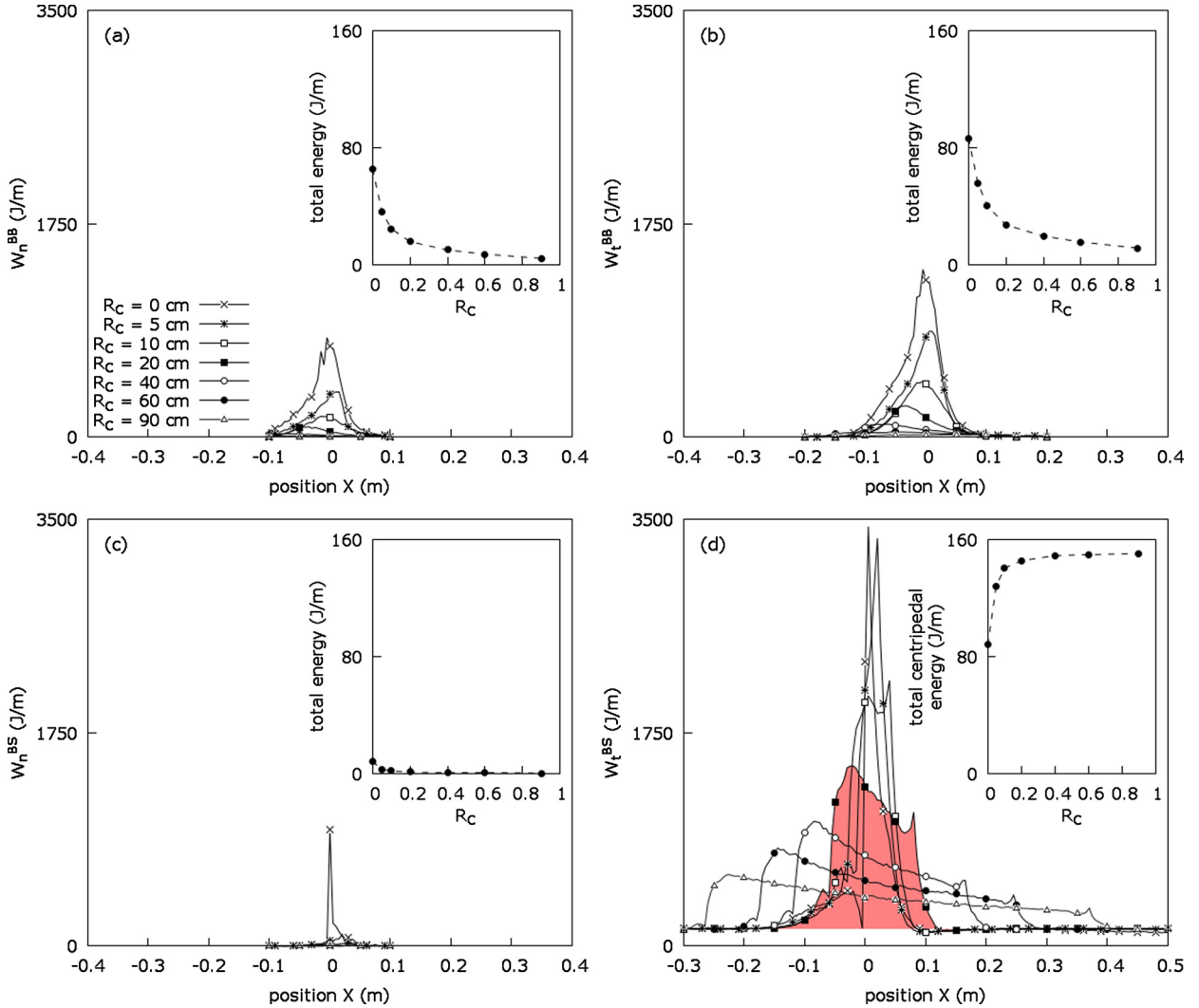


Fig. 7. (Color online.) Dissipated energy around the transition for the tested radii of curvature R_c . The modes of dissipation are distinguished as (a) brick-brick collisions, (b) brick-brick friction, (c) brick-support collisions, and (d) brick-support friction. The insets in the plots (a) to (c) show the energy cumulated on the entire test as a function of the radius R_c . The inset of the plot (d) shows the excessive basal frictional energy, i.e. beyond the constant level of dissipated frictional energy along the slope, which is caused by the centripetal acceleration.

undulations that disturb the flow and allow higher relative velocities between the blocks, both in tangential and normal contact directions. Fig. 6 illustrates this point: the velocity gradient in the direction perpendicular to the slope is clearly higher for a bumpy slope than for a flat one (whatever the aspect ratio of the particles). Consequently, the particle friction is more potent in the flowing mass, particularly in zone 1, as shown in Fig. 5c.

Since nearly 75% of the energy has been lost when the blocks reach the transition zone, the dissipation is lower in this zone, where it is mainly the interparticle friction that has been reduced. This is again a consequence of the more disturbed flow: it makes it more difficult to establish a stationary granular bed that makes the transition smoother. As a result, even if the run-out distance is smaller with a bumpy slope, the isolated blocks go further. This observation is not harmless, especially considering that a single free block in a real rockfall can cause considerable damage.

4.3. Smoothness of a transition

The role of the regularity of the gradient in the transition is regarded by varying the radius R_c of an added curvature tangent to both slopes (Fig. 4c). The rest of the configuration is kept the same as in the reference simulation. Fig. 7 shows how the energy is dissipated around the transition zone for several curvature radii from zero to nearly one meter. The amounts of energy dissipated are computed as the work W by unit of length of the normal or tangential forces—subscripted by n or t respectively—with the support or in-between the particles—superscripted by BS or BB respectively. As shown by the insets in the graphs, the total energy lost by collisions (W_n^{BS} and W_n^{BB} , Figs. 7a and 7c) clearly vanishes in the

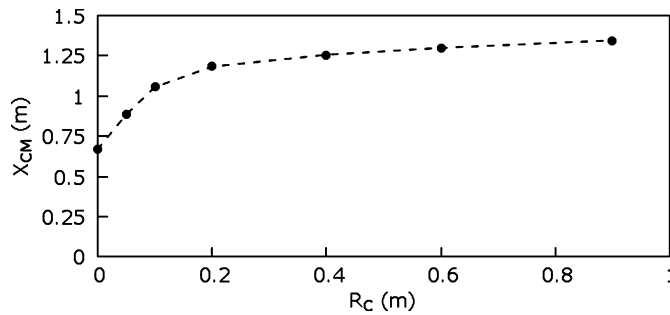


Fig. 8. Position X_{CM} of the deposit mass-center (relative to the position of the slope transition) as a function of the curvature radius R_C .

transition zone as the radius increases. This effect is even more pronounced for collisions with the support that do not significantly dissipate energy from the smallest radius ($R_C = 5$ cm). However, these observations are somehow expected, since increasing the radius makes the transition smoother. For regular slopes and smooth transitional zones, the potential energy was dissipated only by friction at the base of the granular flow, considering frictional parameters greater between blocks than the one between slope and blocks.

If we now look at the dissipation by friction, the case is similar for the friction among particles (W_t^{BB} , Fig. 7b): the total loss of energy declines when R_C is increased. Fig. 7d, corresponding to the friction at the base, shows that the peak of energy declines, but is activated for a longer time. Moreover, the amount of the basal frictional energy loss does not vanish apart from the transition zone, where the density of work W_t^{BS} stabilizes at nearly 120 J/m. Considering that the dissipation level due to friction remains constant along the slope, the excess in dissipation is attributed to the centripetal acceleration that amplifies the force normal to the curvature surface, and thus magnifies the friction force threshold. Somewhat surprisingly, the total amount of energy due to the centripetal acceleration and dissipated by friction of particles on the support, which is a shift of the curve in the inset of Fig. 7d, first begins to increase with R_C and saturates from $R_C = 0.2$ m to a value of the density of work W_t^{BS} at nearly 120 J/m. The initial increase might be explained by a larger flat surface where the particles acquire a better opportunity to slip as R_C increases. The saturation of dissipated energy to a constant value, less obvious to understand, can however be explained quite easily: the curved surface scales with R_C multiplied by the slope angle α , while the gain in the friction force threshold scales with μ/R_C . The friction of a particle sliding from the beginning to the end of the curvature dissipates thus an energy that scales with $\mu \cdot \alpha$, that is a value that does not depend on R_C . The stabilized value is reached from $R_C \simeq 0.2$ m corresponding to the situation where the particles have the possibility to remain in sliding contact with the entire curvature. As a result of the limitation in the energy dissipated, the characteristic lengths of the deposits varies with the same tendency. This is illustrated as an example in Fig. 8 showing the increase of the propagation length of the mass center X_{CM} as a function of R_C .

5. Conclusions

The influence of the geometrical parameters affecting dissipated energy in collisional and frictional modes within a granular flow has been studied by using the discrete element method (DEM). Both trajectory and continuum approaches are ill-posed for the peculiar case of medium-sized rock avalanches and the DEM is a possible alternative. Since DEM experiments allow assessing all data (contact forces, block velocities, etc.) unlike real experiments, their analysis provides a rich source of information for the deep understanding of the rock-flow behavior. The relevance of the numerical model was proven by comparisons with small-scale laboratory experiments. A particular attention was paid for taking into account the realistic shapes of the blocks and to well reproduce the dissipative mechanisms acting within the granular mass or at the base of the flow. The contact parameters were obtained by back analysis of a set of launches of single particles, and the numerical model was successfully validated by laboratory experiments involving an assembly of small bricks flowing down to an inclined plane. Then, the numerical model was used to investigate the influence of geometrical parameters on the dissipative modes involved during the flow.

It has been obtained that the aspect ratio of the particles does not affect so much the run-out and the position of the deposit. However, particle shape strongly changes the way energy is dissipated. In fact, the cubes, which are more likely to roll than to slip, will promote collisional dissipative mechanisms, while the bricks allow the dissipation of energy by friction. Due to their rolling ability, the dispersion of cubes is more spreading.

While traveling on a bumpy terrain, the particle flow was strongly disturbed due to an increase of friction and number of collisions within the flow. As a consequence, the run-out of the deposit was smaller than with a flat slope. Regarding the flow's characteristics, bumpy terrain highly affects the flow, generating a strong vertical velocity gradient. The number and distance of ejected particles, which could be important in the zoning process of rockfall hazard, are also increased due to the granular flow agitation.

Considering a regular transition zone between the two planes, it can be seen that the energy is dissipated mostly by basal friction. The transition zone is subject to an increase in friction forces at the base of the flow due to the centripetal

acceleration. The amount of energy dissipated by these frictional forces does not depend on the bending radius provided that it is large enough compared with the block sizes. For small values of the bending radius, the granular flow was strongly disturbed (collisions and rotation of particles), which makes the frictional effects decline. However, the amount of dissipated energy by collisions and friction within the granular flow increases as the bending radius increases. This leads to a decrease of the run-out distance.

As shown, the geometric parameters have a great influence on the kinematics of the flow and on the dissipative energy modes (by friction or collisions). As a consequence, the results obtained in the present study are highly dependent on the values of the contact parameters chosen. Nevertheless, these results give some useful indications to depict correctly the energy dissipation modes and can provide clues for the derivation of fluid-like models, well used in the engineering of rock. Finally, the discrete element model has to be validated in real case. Probably, new numerical developments need to be done to take into account the rolling resistance mechanism that occurs during shocks between rocks on a soft soil.

References

- [1] P. Habib, Note sur le rebondissement des blocs rocheux, in: Proceedings Meeting on Rockfall Dynamics and Protective Works Effectiveness, 20–21 May 1976, pp. 123–125.
- [2] F. Descoedures, Aspects géomécaniques des instabilités de falaises rocheuses et des chutes de blocs, in: Publications de la Société Suisse de mécanique des sols et des roches, no. 135, Montreux, Switzerland, 7 November 1997.
- [3] S. Evans, O. Hungr, The assessment of rockfall hazard at the base of talus slopes, *Can. Geotech. J.* 30 (1993) 620–636.
- [4] L.K.A. Dorren, F. Berger, U.S. Putters, Real size experiments and 3D simulation of rockfall on forested and non-forested slopes, *Nat. Hazards Earth Syst. Sci.* 6 (2006) 145–153.
- [5] F. Bourrier, L.K.A. Dorren, F. Nicot, F. Berger, F. Darve, Towards objective rockfall trajectory simulation using a stochastic impact model, *Geomorphology* 110 (2009) 68–79.
- [6] S. Wu, Rockfall evaluation by computer simulation, *Transp. Res.* 1031 (1985) 1–5.
- [7] Y. Okura, H. Kitahara, T. Sammori, Fluidization in dry landslides, *Eng. Geol.* 56 (2000) 347–360.
- [8] D. Bozzolo, R. Pamini, Simulation of rock falls down a valley side, *Acta Mech.* 63 (1986) 1–4.
- [9] A. Azzoni, M. De Freitas, Experimentally gained parameters, decisive for rockfall analysis, *Rock Mech. Rock Eng.* 28 (2) (1995) 111–124.
- [10] K. Chau, R. Wong, J. Liu, J. Wu, C. Lee, Shape effects on the coefficient of restitution during rockfall impacts, in: Proc. of the 9th International Congress on Rock Mechanics, vol. 1, International Society for Rock Mechanics (ISRM), Paris, 1999, pp. 541–544.
- [11] M. Fornaro, D. Peila, M. Nebbia, Block falls on rock slopes: application of a numerical simulation program to some real cases, in: Proceedings of the 6th International Congress IAEG, Rotterdam, The Netherlands, 1990, pp. 2173–2180.
- [12] G. Giani, A. Giacomini, M. Migliazza, A. Segalini, Experimental and theoretical studies to improve rock fall analysis and protection work design, *Rock Mech. Rock Eng.* 37 (5) (2004) 369–389.
- [13] B. Heidenreich, Small and half-scale experimental studies of rockfall impacts on sandy slopes, Ph.D. thesis, EPFL, Lausanne, Switzerland, 2004.
- [14] C. Wu, C. Thornton, L. Li, Coefficients of restitution for elastoplastic oblique impacts, *Adv. Powder Technol.* 14 (2003) 937–960.
- [15] F. Ferrari, G.P. Giani, T. Apuani, Why can rockfall normal restitution coefficient be higher than one?, *Rend. Online Soc. Geol. It.* 24 (2013) 122–124.
- [16] O. Hungr, A model for the runout analysis of rapid flow slides, debris flows, and avalanches, *Can. Geotech. J.* 32 (4) (1995) 610–623, <http://dx.doi.org/10.1139/t95-063>.
- [17] A. Voellmy, Über die zerstörungskraft von Lawinen, *Schweiz. Bauztg.* 73 (1955) 212–285.
- [18] A. Mangeney-Castelnau, J.-P. Vilotte, M.O. Briseau, B. Perthame, F. Bouchut, C. Simeoni, S. Yerneni, Numerical modeling of avalanches based on Saint Venant equations using a kinetic scheme, *J. Geophys. Res.* 108 (B11) (2003) 2527, <http://dx.doi.org/10.1029/2002JB002024>.
- [19] M. Pirulli, A. Mangeney, Results of back-analysis of the propagation of rock avalanches as a function of the assumed rheology, *Rock Mech. Rock Eng.* 41 (1) (2008) 59–84, <http://dx.doi.org/10.1007/s00603-007-0143-x>.
- [20] K. Hutter, T. Koch, C. Plüss, S.B. Savage, The dynamics of avalanches of granular-materials from initiation to runout. 2. Experiments, *Acta Mech.* 109 (1995) 127–165, <http://dx.doi.org/10.1007/BF01176820>.
- [21] C. Sautier, V. Labiouse, M. Pirulli, C. Scavia, J. Zhao, Numerical simulation of gravel unconstrained flow experiments: a comparison between dan-3D and rash-3D codes, in: European Rock Mechanics Symposium EUROCK, 15–18 June 2010, pp. 571–574.
- [22] M. Pirulli, The Thurwieser rock avalanche (Italian Alps): description and dynamic analysis, *Eng. Geol.* 109 (1, 2) (2009) 80–92.
- [23] C. Campbell, P. Cleary, M. Hopkins, Large-scale landslide simulations of global deformation, velocities and basal friction, *J. Geophys. Res., Solid Earth* 100 (1995) 8267–8283.
- [24] F. Calvetti, G.B. Crosta, M. Tatarella, Numerical simulation of dry granular flows: from the reproduction of small-scale experiments to the prediction of rock avalanches, *Riv. Ital. Geotec.* 2 (2000) 1–38.
- [25] P.W. Cleary, M. Prakash, Discrete-element modeling and smoothed particle hydrodynamics: potential in the environmental sciences, *Philos. Trans. R. Soc., Math. Phys. Eng. Sci.* 362 (2004) 2003–2030, <http://dx.doi.org/10.1098/rsta.2004.1428>.
- [26] L. Staron, Mobility of long-runout rock flows: a discrete numerical investigation, *Geophys. J. Int.* 172 (2008) 455–463, <http://dx.doi.org/10.1111/j.1365-246X.2007.03631.x>.
- [27] R. Valentino, G. Barla, L. Montrasio, Experimental analysis and micromechanical modelling of dry granular flow and impacts in laboratory flume tests, *Rock Mech. Rock Eng.* 41 (2008) 153–177, <http://dx.doi.org/10.1007/s00603-006-0126-3>.
- [28] A. Taboada, N. Estrada, Rock-and-soil avalanches: theory and simulation, *J. Geophys. Res.* 114 (2009), <http://dx.doi.org/10.1029/2008JF001072>.
- [29] J. Banton, P. Villard, D. Jongmans, C. Scavia, Two-dimensional discrete element models of debris avalanches: parameterization and the reproducibility of experimental results, *J. Geophys. Res.* 114 (2009) F04013, <http://dx.doi.org/10.1029/2008JF001161>.
- [30] K.J. Chang, A. Taboada, Discrete element simulation of the Jiufengershian rock-and-soil avalanche triggered by the 1999 Chi-Chi earthquake, Taiwan, *J. Geophys. Res.* 114 (2009) F03003, <http://dx.doi.org/10.1029/2008JF001075>.
- [31] P.A. Cundall, O.D.L. Strack, A discrete numerical-model for granular assemblies, *Geotechnique* 29 (1979) 47–65.
- [32] O.R. Walton, R.L. Braun, Viscosity, granular temperature, and stress calculations for shearing assemblies of inelastic, frictional disks, *J. Rheol.* 30 (1986) 949–980.
- [33] L. Favier, D. Daudon, F. Donze, J. Mazars, Predicting the drag coefficient of a granular flow using the discrete element method, *J. Stat. Mech. Theory Exp.* (2009) 1–15, <http://stacks.iop.org/JSTAT/2009/P06012>.
- [34] F. Alonso-Marroquin, Spheropolygons: a new method to simulate conservative and dissipative interactions between 2d complex-shaped rigid bodies, *Europhys. Lett.* 83 (1) (2008), <http://dx.doi.org/10.1209/0295-5075/83/14001>.
- [35] V. Richefeu, G. Mollon, D. Daudon, P. Villard, Dissipative contacts and realistic block shapes for modelling rock avalanches, *Eng. Geol.* 149–150 (2012) 78–92, <http://dx.doi.org/10.1016/j.enggeo.2012.07.021>.

- [36] G. Mollon, V. Richefeu, P. Villard, D. Daudon, Numerical simulation of rock avalanches: influence of local dissipative contact model on the collective behavior of granular flows, *J. Geophys. Res.* 117 (2012) F02036, <http://dx.doi.org/10.1029/2011JF002070>.
- [37] G. Van Den Bergen, *Collision Detection in Interactive 3D Environments*, The Morgan Kaufmann Series in Interactive 3D Technology, Morgan Kaufmann Publishers, 2004, p. 280.
- [38] I. Manzella, V. Labiose, Flow experiments with gravel and blocks at small scale to investigate parameters and mechanisms involved in rock avalanches, *Eng. Geol.* 109 (2009) 146–158.
- [39] D.D. Durda, N. Movshovitz, D.C. Richardson, E. Asphaug, A. Morgan, A.R. Rawlings, C. Vest, Experimental determination of the coefficient of restitution for meter-scale granite spheres, *Icarus* 211 (2010) 849–855, <http://dx.doi.org/10.1016/j.icarus.2010.09.003>.
- [40] R. Ramírez, T. Pöschel, N.V. Brilliantov, T. Schwager, Coefficient of restitution of colliding viscoelastic spheres, *Phys. Rev. E* 60 (4) (1999) 4465.
- [41] R. Sondergaard, K. Chaney, C.E. Brennen, Measurements of solid spheres bouncing off flat plates, *J. Appl. Mech. (ISSN 0305-0548)* 112 (3) (1990) 694–699.
- [42] L. Labous, A.D. Rosato, R.N. Dave, Measurement of collisional properties of spheres using high-speed video analysis, *Phys. Rev. E, Stat. Phys. Fluids Relat. Interdiscip. Topics* 56 (2000) 5717–5725.
- [43] G. Kuwabara, K. Kono, Restitution coefficient in a collision between two spheres, *J. Appl. Phys.* 26 (1987) 1230–1233.
- [44] C.K.K. Lun, S.B. Savage, The effects of an impact velocity dependent coefficient of restitution on stresses developed by sheared granular materials, *Acta Mech.* 63 (1986) 15–44.